ELT M4 Adaptive Mirror Actuator: Magnetic Optimization and Future Developments

C. Del Vecchio[1], R. Briguglio[1], M. Xompero[1], A. Riccardi[1], G. Agapito[1], S. Barmada[2], L. Sani[2], R. Biasi[3], D. Gallieni[4]

[1]OAA, National Institute for Astrophysics, Firenze, Italy
[2]DESTEC, Università degli Studi di Pisa, Pisa, Italy
[3]Microgate Srl, Bolzano, Italy
[4]ADS International Srl, Valmadrera (LC), Italy

Abstract:

The quaternary mirror (M4) of the Extremely Large Telescope will be equipped with an Adaptive Optics Unit, in order to compensate the effects of the atmospheric turbulence. The highly accurate, closed loop actuation of the thin mirror is provided by 5316 contactless actuators. Their core is a voice-coil device, whose magnetic design exploits the concept adopted in all previous units. As some implementation details were changed to deal with the challenges imposed by the performances of the M4 unit, in the present paper we discuss the optimization design of the magnetic circuit carried out by means of Comsol, as well as the possible, future study of the dynamic magneto-mechanical behaviour when operating in open and closed loop.

The previous actuators, equipping the LBT, VLT, and Magellan telescopes, are demonstrating to fully accomplish the very demanding task of the turbulence correction. The day-to-day experience gained through the use of those units has allowed to point out possible improvements, in order to increase the efficiency of the actuator and its dynamic response. The role played by the various factors potentially able to enhance the performances of the device are analyzed in this paper, in terms of materials and geometry of the magnetic general arrangement.

The optimization process allows to increase by approximately 20% the efficiency of the proposed geometry with respect to the LBT and VLT ones, while the preliminary, multi-physics dynamic runs make it possible to anticipate some rather interesting capabilities in terms of closed loop performances.

Keywords: Adaptive Optics, Magnetostatics, E-ELT, Deformable Mirrors, Voice-coil Actuators

1 Introduction

The atmospheric turbulence affecting the telescope optics is corrected by the Adaptive Optics (AO) system by means of deformable optical surfaces. At the Large Binocular Telescope (LBT) and the Very Large Telescope (VLT) the deformations are actuated by voice-coil actuators, which provide a magnetic force generated by the interaction between a coil embedded in the Reference Frame (RF) and a permanent magnet (PM) assembly, glued to the non-active surface of the deformable mirror (DM), mechanically decoupled with respect to the RF (see Riccardi et al. [2008] and Gallieni and Biasi [2013]).

The experience gained through the use of those units has allowed to point out possible improvements when designing the the quaternary mirror (M4) of the Extremely Large Telescope (ELT), equipped with an Adaptive Optics unit, aimed at compensating the effects of the atmospheric turbulence with 5316 contactless actuators (see Biasi et al. [2016] and Vernet et al. [2012]).

The magnetic circuit of the M4 actuator, conceptually similar to the LBT and the VLT ones, consists of an inner and outer PMs — both of them split into 8 sectors — , and a coil, coaxial with the magnets. The magnetization of each sector lie in the plane of symmetry of the sector itself, perpendicular to the axis of the inner, cylindri-

cal magnet, axially magnetized, at an angle β with respect to the normal to that axis. Approximating the octagonal prism of the outer magnet with a circular hollow cylinder — suitable for a 2d axisymmetric geometry, as all the other components — doesn't affect significantly the accuracy of the results. The geometry and the most relevant specifications of the actuator, schematized in in Fig. 1 as a main (outer) magnet, a bias (inner) magnet, a coil, and an iron *pot*, are summarized in in Tab. 1.

The Comsol model has been built with all the above mentioned geometrical components, adding a semi-circular air domain with an infinite element layer, and meshed with approximately 5500 elements, in order to obtain accurate results.

In the most general case, the power P supplied by the generator in an electromechanical device, whose resistance is R, delivering the current I is the sum of the *resistive* power RI^2, the *inductive* power $\frac{d\Phi}{dt}I$, and the thermal losses Q:

$$P = RI^2 + \frac{d\Phi}{dt}I + Q \tag{1}$$

As the time derivative of the concatenated flux $\Phi = \Phi(z, I)$ is defined in Eq. 2,

$$\frac{d\Phi}{dt} = \frac{\partial\Phi}{\partial I}\frac{dI}{dt} + \frac{\partial\Phi}{\partial z}\frac{dz}{dt} \tag{2}$$

where $L = \frac{\partial\Phi}{\partial I}$ is the inductance and $K_{bemf} = \frac{\partial\Phi}{\partial z}$ is the *back electromotive force* function, the induced voltage V_i, obtained dividing $P - RI^2$ by I in Eq. 1, is

$$V_i = L\frac{dI}{dt} + K_{bemf}\frac{dz}{dt} + \frac{Q}{I} \tag{3}$$

Because K_{bemf} is equal to the force function $K_f = \frac{F}{I}$, and the time derivative of the kinetic energy $F\frac{dz}{dt}$ is $K_f I\frac{dz}{dt}$, Eq. 1 can be rewritten as

$$P = RI^2 + L\frac{dI}{dt}I + Q + F\frac{dz}{dt} \tag{4}$$

Because of the very demanding thermal specifications of the telescope environment, the term Q in Eq. 4 must be accurately evaluated, in contrast to most of the electric motors, so that the power balance is crucial when dealing with the dynamic response of the system.

outer mag radii	2.1 6.1 mm
inner mag radius	2 mm
mag height	4.2 mm
coil radii	2.3 7.4 mm
coil height	3.3 mm
rms force (turbulence correction)	.363 N
max force (static)	.36 N
max force (dynamic)	1.27 N
stroke (mechanical)	±200 µm
gap (magnet-to-coil)	400 µm
bandwidth	1 kHz
typical inter-actuator spacing	26 mm
typical mobile mass	≤ 10 g

Table 1: Specifications of the actuator.

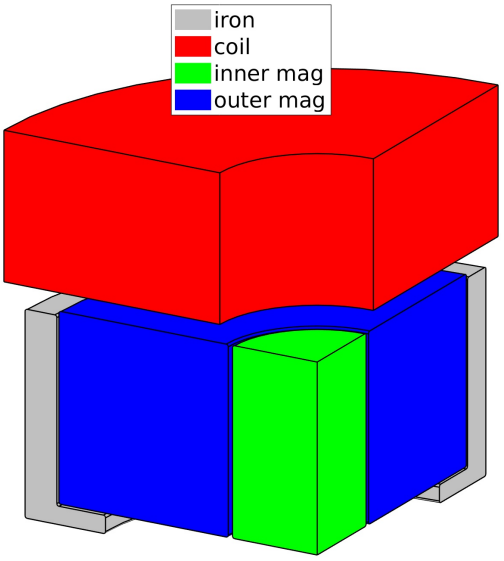

Figure 1: A schematic view of the actuator.

2 Optimization

According to Del Vecchio et al. [2008], the efficiency of a voice-coil actuator, that is the ratio of the the force F to the square root of the power P, $\varepsilon = \frac{F}{\sqrt{P}}$ and the force function K_f, described in Sec. 1, are defined as in Equations 5 and 6, respectively, where S is the cross section of the coil, whose mean

radius is $\overline{R}$ consisting of N wires of section s and conductivity ρ, $\gamma = \dfrac{Ns}{S}$ is the filling factor, and $\Psi = \dfrac{\int_S B_r \, r \, dA}{S}$, where B_r is the radial component of the magnetic flux density $\mathbf{B}$. As, given ρ and γ, ε depends linearly on Ψ, we have analyzed the following three methods able to increase Ψ: a better PM material, a non-radial magnetization direction of the main magnet, and the addition of an iron *pot*. In particular, we have selected three soft iron materials — the C40, the Euronorm FeV 270 50H, and a high-permeability steel produced by Sumitomo — and three PM materials — the 48H and the 55 produced by Arnold and the Vacodym 510R, produced by Vacuumschmelze — the one selected for the LBT and VLT telescopes. For all the above mentioned material combinations, we have computed ε as a function of the magnetization angle β: all the materials exhibit a maximum of $\varepsilon = \varepsilon(\beta)$ of $\approx 1\,\mathrm{N} \times \sqrt{\mathrm{W}}$, and the addition of the iron *pot* increases by few % the efficiency delivered by the PM compound. Choosing the Arnold 48 PM for the PM, the maximum efficiency is $.996\,\mathrm{N} \times \sqrt{\mathrm{W}}$ at $\beta = 38.2°$; adding the C40 iron, we obtain a maximum efficiency of $1.036\,\mathrm{N} \times \sqrt{\mathrm{W}}$ at $\beta = 38.7°$, as shown in Fig. 2.

$$\varepsilon = \sqrt{2\pi \frac{\gamma}{\rho} \frac{S}{\overline{R}}} \; \Psi \tag{5}$$

$$K_f = N \, 2\pi \, \Psi \tag{6}$$

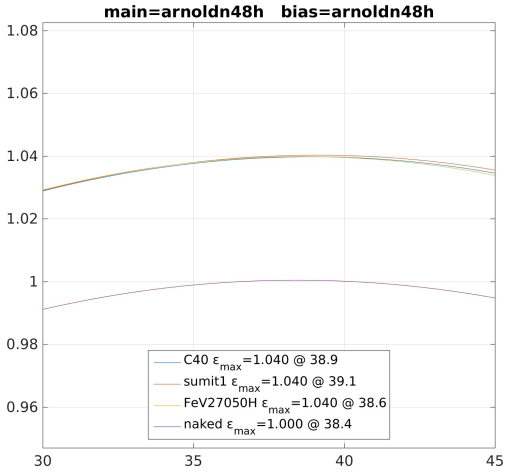

Figure 2: The optimization process.

3 Statics

In principle, the main parameter affecting the efficiency — the variable Ψ in Eq. 5 — depends on the current I flowing through the coil, because the relative permeability of the PM isn't equal to 1. Nevertheless, as in our case $I \leq 1\,\mathrm{A}$, the flux of $\mathbf{B}$ in the coil is mostly given by the magnets, as shown in Figures 3 and 4 for a a model with and without iron, respectively. Moreover, also the force function[1] K_f, described in Sec. 1 and defined in Eq. 6, doesn't depend on I for $I \leq 1\,\mathrm{A}$, and is equal to $3.547\,\mathrm{N} \times \mathrm{A}^{-1}$.

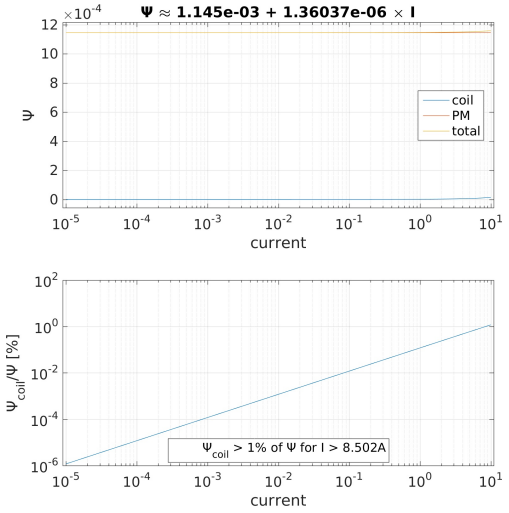

Figure 3: Φ as a function of I with iron.

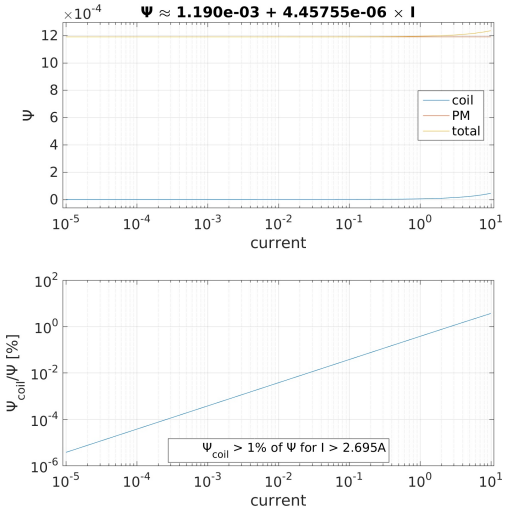

Figure 4: Φ as a function of I without iron.

[1] Due to the low values of I and z, K_f (and, as a consequence, K_{bemf} in Eq. 3) are almost always regarded as constants here and in the following dynamic analysis.

In order to evaluate the inductance of the magnetic circuit, the model set to evaluate the static response has been run with a time-dependent study, replacing the constant current with a polynomial $I = I(t)$ from $t = 0$ to $t = t_s$, continuous up to the fourth derivative, with $I(0) = 0$ and $I(t_s) = I^\star$ (cf. Eq. 9). Parametrically solving for various $I^\star$ and z — the displacement of the moving domains, namely the magnets and the iron — the inductance is computed as the ratio $\frac{V - IR}{\frac{dI}{dt}}$. The results, summarized in Fig. 5, show that the inductance is from 2.9% to 3.5% and from .67% to .82% larger that the inductance of the pure coil, equal to 1.744 mH, with and without iron, respectively.

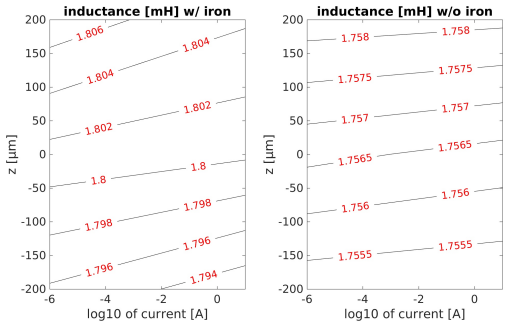

Figure 5: The inductance as a function of I and z.

4 Dynamics

Defining the Comsol *Moving mesh* as well as the Ordinary Differential Equations (*ODE*) allows to study the actuator dynamics, with the aim of computing the total power needed to deliver a certain closed-loop motion. The power budget must consider the heating due to the eddy currents growing in the magnets and in the iron, whose ρ isn't negligible. The default Comsol definition of the induced voltage in the *Homogenized multi-turn* coil cannot take into account the power dissipated by those currents, so that the definition of the concatenated flux in the coil has been reformulated as $\Phi = \Phi_c + \Phi_q$, where Φ_c, defined in Eq. 7, where A_φ is the φ component of the magnetic vector potential $\mathbf{A}$, and Φ_q, defined in Eq. 8 (cf. Eq. 3), takes into account the thermal losses in the magnets and in the iron — the surface integration of the product of the current densities J_φ times the electric field E_φ is to be carried out on each j surface of the magnets and the iron.

$$\Phi_c = 2\pi \frac{N}{S} \int_S A_\varphi r dS \tag{7}$$

$$\Phi_q = \frac{2\pi}{I} \int_{S_j} J_\varphi E_\varphi r dS \tag{8}$$

After verifying that definitions in an open-loop test (Sec. 4.1), we have run the model in a closed-loop system (Sec. 4.2). In both cases, the (basically constant) inductance can be evaluated as discussed in Sec. 3.

4.1 Open loop

Fig. 6 shows the open loop power budget when feeding the coil with the current $I(t) = I_s \Gamma(t)$, where the *smoothed* step function $\Gamma(t)$ — a function continuous of to its fourth derivative for $t \geq 0$ — is defined in Eq. 9, with $t_s = 5\,\text{ms}$ and $I_s = 5\,\text{mA}$. Besides verifying that the power balance is satisfied, Fig. 6 reveals that for velocities $\geq .035\,\text{m} \times \text{s}^{-1}$ the thermal losses are $> 12\%$ and $> 2.2\%$ of the total power with and without iron, respectively.

$$\Gamma(t) = \begin{cases} -\frac{t^4 \left(20\,t^3 - 70\,t^2\,t_s + 84\,t\,{t_s}^2 - 35\,{t_s}^3\right)}{{t_s}^7} & \text{if } 0 \leq t \leq t_s \\ 1 & \text{if } t > t_s \end{cases} \tag{9}$$

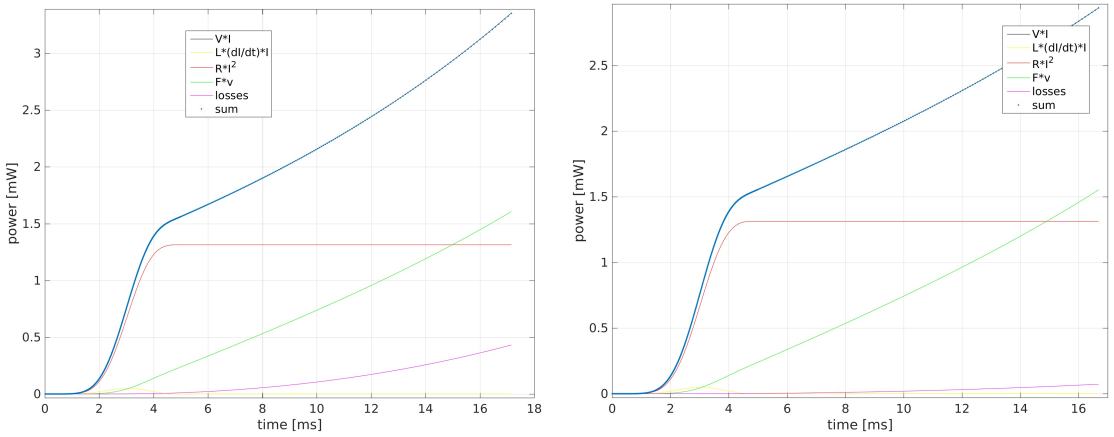

Figure 6: The open loop power budget with (left) and without (right) iron.

4.2 Closed loop

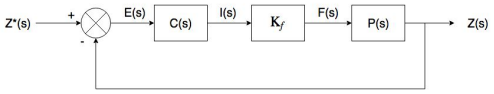

Figure 7: The closed loop block diagram.

In order to evaluate the actual dynamic capabilities of the actuator, the coil of the model described in Sec. 4.1 has been fed with the current defined in Eq. 10, where

$$I(t) = K_p\epsilon(t) + K_d\frac{d\epsilon(t)}{dt} + K_i\int_0^t \epsilon(t)dt \quad (10)$$

$\epsilon(t) = z^\star(t) - z(t)$ is the difference between the function $z^\star(t) = z_s\Gamma(t)$, where $\Gamma(t)$ is defined in Eq. 9 and z_s is the desired set point (stroke), and the actual position $z(t)$. The parameters of the very simple PID controller of Eq. 10, depicted in Fig. 7, have been selected as the best results, in terms of steady-state error and stability, of a Matlab® run spanning wide ranges of K_p, K_d, and K_i, with $K_f = 3.547\,\mathrm{N}\times\mathrm{A}^{-1}$, according to the result in Sec. 2[2]. In Fig. 7, $C(s) = K_p + sK_d + \frac{1}{s}K_i$ identifies the Laplace transform of the controller (Eq. 10) and $P(s) = (m+m_o)\,s^2 + cs + k$ identifies the Laplace transform of the plant, $(m+m_o)\,\frac{d^2z}{dt^2} + c\frac{dz}{dt} + kz$, where $m = 5.003$ or $3.787\times10^{-3}\,\mathrm{kg}$ is the mobile mass (computed by Comsol with and without iron, respectively) of the actuator, $m_0 = .001\,\mathrm{kg}$ is the portion of the glass mass moved by the actuator (cf. Tab. 1), $c = 10\,\mathrm{N}\times\mathrm{s}\times\mathrm{m}^{-1}$ is the viscous damping coefficient in the air gap, and $k = 1\times10^6\,\mathrm{N}\times\mathrm{m}^{-1}$ is the typical glass stiffness when actuating a single stroke. Fig. 8 shows $\epsilon(t)$ and $I(t)$ for $t_s = .8\,\mathrm{ms}$, $z_s = 1\,\mu\mathrm{m}$, $K_p = 3.5\times10^7\,\mathrm{A}\times\mathrm{m}^{-1}$, $K_d = 600\,\mathrm{A}\times\mathrm{s}\times\mathrm{m}^{-1}$, and $K_i = 1\times10^{10}\,\mathrm{A}\times\mathrm{m}^{-1}\times\mathrm{s}^{-1}$. The steady-state current is $.752\,\mathrm{A}$ with iron, and $.781\,\mathrm{A}$ without iron, because of the (slightly) lower efficiency of the latter. The steady-state z errors are 0.752% and 0.781%, respectively. Fig. 9 shows the power budget of the closed loop response. Although the thermal losses of the model without iron are slightly lower than the ones with the iron, as expected, the two power budgets are practically indistinguishable.

[2] This simplification allows to define to PID parameter implemented in the Comsol model with an error band $\leq 1\%$. Although even a better response can be obtained with more refined controllers, such an assumption is very satisfactory, as the design of the control system isn't a topic of this paper.

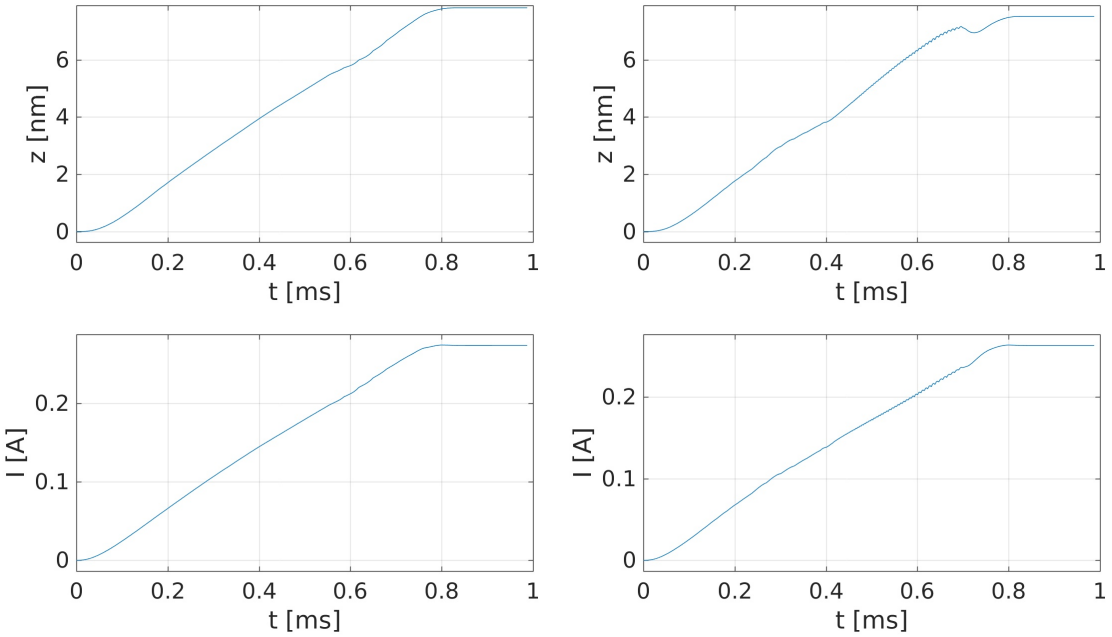

Figure 8: The closed loop response in terms of error and current with (left) and without (right) iron.

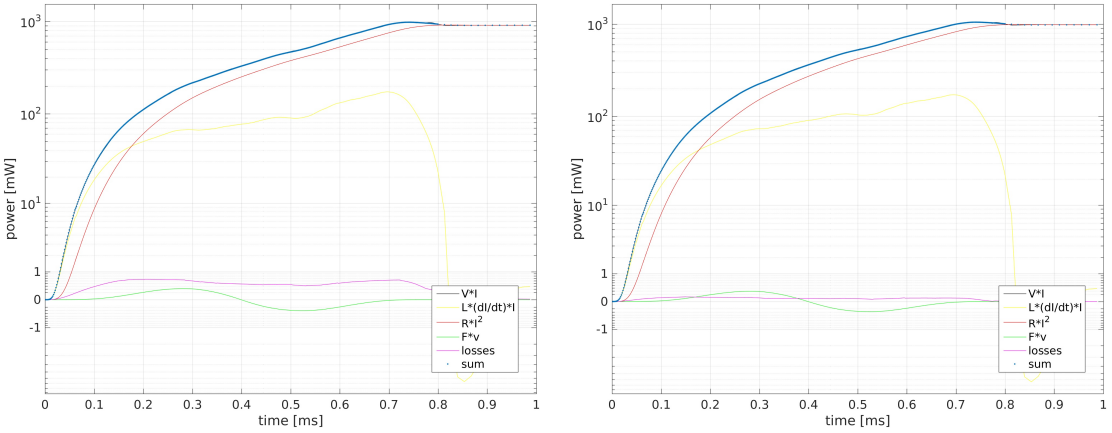

Figure 9: The closed loop power budget with (left) and without (right) iron.

5 Conclusions

The performances of the current AO units have been excellent through the past years. Nevertheless, the more challenging requirements of the ELT goals demand further improvements of the actuating system of the DM. This paper shows how to fulfill those specifications. The optimization of the magnetic circuit of the actuator shows that properly orientating the magnetization directions, along with some minor material and geometry revisions, allows to reach an efficiency $\geq 1\,\mathrm{N} \times \mathrm{W}^{-\frac{1}{2}}$. Two Comsol tools, the deformable mesh and the ODE algorithms, allow a complete definition of the dynamics of the system. Provided that the induced voltage is properly defined, the total power — a crucial parameter in terms of optical stability — is correctly computed. As such a power balance is verified via some open-loop dynamic simulations, we have tested the model with some preliminary closed-loop runs, whose results are quite satisfactory: with a very simple PID controller the actuator can command a stroke of the order of 1 µm in .8 ms. The proposed method is a valuable tool to implement more refined control strategies for actuating with great accuracy the very fast corrections of high spatial-density, large deformable mirrors.

References

R. Biasi, M. Manetti, M. Andrighettoni, G. Angerer, D. Pescoller, C. Patauner, D. Gallieni, M. Tintori, M. Mantegazza, P. Fumi, P. Lazzarini, R. Briguglio, M. Xompero, G. Pariani, A. Riccardi, E. Vernet, L. Pettazzi, P. Lilley, and M. Cayrel. E-ELT M4 adaptive unit final design and construction: a progress report. In *Adaptive Optics Systems III*, volume 9909, pages 9909 – 9909 – 16, 6 2016. doi: 10.1117/12.2234735. URL `https://doi.org/10.1117/12.2234735`.

C. Del Vecchio, A. Riccardi, F. Marignetti, R. Biasi, D. Gallieni, and R. Spairani. Linear motors for astronomical mirrors. In *Industry Applications Society Annual Meeting, 2008. IAS '08. IEEE*, pages 1–8, 10 2008. ISBN 978-1-4244-2278-4. doi: 10.1109/08IAS.2008.45.

D. Gallieni and R. Biasi. The new VLT-DSM M2 unit: construction and electromechanical testing. In S. Esposito and L. Fini, editors, *Third AO4ELT Conference*, Proc. AO4ELT. AO4ELT, 5 2013. doi: 10.12839/AO4ELT3.17883.

A. Riccardi, M. Xompero, D. Zanotti, L. Busoni, C. Del Vecchio, P. Salinari, P. Ranfagni, G. Brusa Zappellini, R. Biasi, M. Andrighettoni, D. Gallieni, E. Anaclerio, H. M. Martin, and S. M. Miller. Adaptive secondary mirror for the Large Binocular Telescope: results of acceptance laboratory test. In C. E. Max, P. L. Wizinowich, and N. Hubin, editors, *Adaptive Optics Systems*, volume 7015 of *Proc. SPIE*, pages 12.1–12.9. SPIE, 6 2008.

E. Vernet, M. Cayrel, N. Hubin, M. Mueller, R. Biasi, D. Gallieni, and M. Tintori. Specifications and design of the E-ELT M4 adaptive unit. In *Adaptive Optics Systems III*, volume 8447, pages 8447 – 8447 – 8. SPIE, 7 2012. doi: 10.1117/12.925133. URL `https://doi.org/10.1117/12.925133`.